American Journal of Engineering Research (AJER) 2020
American Journal of Engineering Research (AJER)
e-ISSN: 2320-0847 p-ISSN : 2320-0936
Volume-9, Issue-4, pp-171-180
www.ajer.org
Research Paper Open Access

Modified Contact Constraints in Sphere-Based 3-D DDA

S. Amir Reza Beyabanaki[1], Amvrossios C. Bagtzoglou[2]
[1]*McMillen Jacobs Associates, Walnut Creek, CA, USA*
[2]*Department of Civil and Environmental Engineering, University of Connecticut, Storrs, CT, USA*

ABSTRACT:
In 2012, a new numerical model, called sphere-based 3-D DDA, for simulation of granular materials consisting of 3-D spheres was presented by the authors (Beyabanaki and Bagtzoglou [1]). In the existing sphere-based 3-D DDA methodand in studies performed by other researches,the penalty method is used to enforce sphere contact constraints. Although thisapproach is fairly simple to implement, it can lead to inaccuracies that may be large for small values of the penalty number.Moreover, this method creates sphere contact overlap that may violate the physical constraints. In this study, the augmented Lagrangian method is used to overcome these limitations. For this purpose, contact constraints in sphere-based 3-D DDAare modifiedandthe corresponding formulations are presented.The modified contact constraints have been implemented into a sphere-based 3-D DDA numerical codeand two test cases are studied inorder to verify the formulations. The results show the capability of the modified sphere-based 3-D DDA.

KEYWORDS: *sphere-baseddiscontinuous deformation analysis, contact constraints, augmented Lagrangian method, Penalty method, numerical method.*

Date of Submission: 03-04-2020 Date of acceptance: 19-04-2020

I. INTRODUCTION

Discontinuous Deformation Analysis (DDA) is a displacement-based method that was originally developed by Shi [2, 3] for modeling large deformation in fractured rock masses. DDA provides a useful tool to analyze the mechanical response of discrete blocks. Several studies have been conducted to validate and develop this numerical approach. Applications of the DDA in rock mechanics and rock engineering are reviewed by Jing and Hudson [4], Jing [5], and Ohnishi and Nishiyama [6]. In a comprehensive study, MacLaughlin and Doolin [7] reviewed more than 100 validation studies on the DDA. Moreover, Shi [8] presented applications of the DDA to rock stability analysis. Applications of the DDA to model slopes and underground openings are also reviewed by Hatzor and Bakon-Mazor [9].

Basic formulations of matrices for different potential terms are presented in detail by Shi [10] and Wu et al. [11]. Applications of 3-D DDA were demonstrated by Liu et al. [12] and Yeung et al. [13, 14]. As the first step in developing 3-D DDA, its contact model was presented and, for this purpose, a point-to-face model for contacts between polyhedral blocks in 3-D DDA was developed by Jiang and Yeung [15]. Also, Wu et al. [16] developed a new contact searching algorithm for frictionless vertex-to-face contact problems. Moreover, Yeung et al. [17] and Wu [18] presented different algorithms for edge-to-edge contacts. Finally, a new algorithm to search and calculate geometrical contacts in 3-D was presented by Beyabanaki et al. [19]. Ahn and Song [20] presented a new contact definition algorithm for 3-D DDA. As the next step, block deformability in 3-D DDA was improved by Beyabanaki et al. [21, 22] who implemented 8-node and 20-node hexahedral isoparametric finite elements into 3-D DDA. Furthermore, as an alternative method to improve block deformability in 3-D DDA, high-order displacement functions were used by Beyabanaki et al. [23, 24]. Finally, validation and application of 3-D DDA with tetrahedron finite element meshed block were presented by Liu et al. [25]. Before using a method for a dynamic problem, it should be demonstrated that the method is able to model dynamic conditions. For this purpose, Beyabanaki et al. [26] compared the 3-D DDA solution for dynamic block displacement with analytical solutions to study the validity of the method in order to show the capability of polyhedral-based 3-D DDA to model dynamic problems. Moreover, Bakun-Mazor et al. [27] validated 3-D DDA by comparing the numerical results obtained for modeling dynamic, single, and double face sliding of a block with their proposed analytical solution. 3-D DDA was coupled with smoothed particle hydrodynamics by

Zhang et al. [28] to study the geological phenomena associated with fluid-solid interaction. Zhu et al. [29] integrated 3-D DDA with binocular photogrammetry and evaluated the stability of tunnels in jointed rock masses. To address rock-cutting and rock-penetration problems, Zhao et al. [30] coupled 3-D DDA with a distinct lattice spring model. Zhang et al. [31] constructed new types of 3-D DDA slope models with GIS techniques and Liu et al. [32] analyzed the velocity distribution and the key point displacements of the brick masonry buildings using 3-D DDA. Recently, Beyabanaki [33] reviewed applications of 3-D DDA.

Relatively little work on the development of the DDA in particulate media has been published. Disk-based DDA in 2-D to model particulate media was presented by Ke and Bray [34]. Rein and Andrés [35] used the method to model granular transport in vibrating feeders. The ability of the DDA to model the response of systems of disks was presented by Thomas and Bray [36], Thomas [37], and Koyama et al. [38]. Beyabanaki and Bagtzoglou[1, 39] presented a new formulation of sphere-based 3-D DDA. The same authors presented a disk-based 2-D DDA with a new contact model (Beyabanaki and Bagtzoglou [40]) and investigated the accuracy of dynamic disk-based DDA (Beyabanaki and Bagtzoglou [41]). Beyabanaki et al. [42] successfully applied disk-based DDA to simulate the Donghekou landslide triggered by the Wenchuan earthquake. A friction contact model in sphere-based 3-D DDA was presented by Huang et al. [43]. Wang et al. [44] presented a new sphere-to-edge contact for sphere-based 3-D DDA. Recently, discontinuous deformation analysis for ellipsoids using cone complementary formulation was presented by Fan et al. [45].

The penalty method was used in the sphere-based 3-D DDA studies to enforce contact constraints at the sphere interface. The accuracy of the contact solution depends highly on the choice of the penalty number, and the optimal number cannot be explicitly found beforehand. A very high penalty number leads to progressive ill-conditioning of the resulting system, and low value leads to overlaps between spheres or spheres and boundaries. Therefore,high-accuracy solutions may not be obtained using this method.

The Augmented Lagrangian Method (ALM) is a well-known method to overcome these problems for equality constrained problems [46]. In this study, contact constraints are enforced in sphere-based 3-D DDA using this method. Two illustrative examples are presented to demonstrate this new approach.

II. SPHERE-BASED 3-D DDA

Sphere-based 3-D DDA is an implicit technique, and involves formulation and solution of a system of simultaneous equilibrium equations. In this method, the total potential energy is the summation of all potential energy sources for each sphere, which involves the potential energy contributed by the point loads on a sphere, inertia forces, volume forces, fixed points, and potential energy when the spheres contact each other.

Assuming that the spheres are rigid, the relation between them can be presented as below[1]:

$$\begin{Bmatrix} u \\ v \\ w \end{Bmatrix} = [T_i(x,y,z)].\{D_i\} \tag{1}$$

where

$$[T_i(x,y,z)] = \begin{pmatrix} 1\ 0\ 0\ 0\ (z-z_0) & -(y-y_0) \\ 0\ 1\ 0\ -(z-z_0)\ 0\ (x-x_0) \\ 0\ 0\ 1\ (y-y_0) & -(x-x_0)\ 0 \end{pmatrix} \tag{2}$$

and

$$\{D_i\}^T = \{u_0 v_0 w_0 r_x r_y r_z\} \tag{3}$$

(x_0, y_0, z_0) are the coordinates of the sphere center, and (u_0, v_0, w_0) represents rigid body translations; (r_x, r_y, r_z) indicates the rotation angles in radians of sphere i with a rotation centre at (x_0, y_0, z_0). $[T_i(x,y,z)]$ is the first order displacement function, and $\{D_i\}$ is the vector of displacements of sphere i in three dimensions.

To eliminate the possibility for the error of free expansion under rigid body rotation, the exact solution for the displacements can be used to compute the components of (u,v,w) due to (r_x, r_y, r_z) by extending the following rigid body rotation:

$$\begin{cases} u = u_0 + (x - x_0)(\cos r_z - 1) - (y - y_0)\sin r_z \\ +(z - z_0)\sin r_y + (x - x_0)(\cos r_y - 1) \\ v = v_0 + (x - x_0)\sin r_z + (y - y_0)(\cos r_z - 1) \\ +(y - y_0)(\cos r_x - 1) - (z - z_0)\sin r_x \\ w = w_0 + (z - z_0)(\cos r_y - 1) - (x - x_0)\sin r_y \\ +(y - y_0)\sin r_x + (z - z_0)(\cos r_x - 1) \end{cases} \quad (4)$$

The total potential energy for an N spheres system can be expressed in matrix form as follows:

$$\begin{bmatrix} [K_{11}][K_{12}][K_{13}]\dots[K_{1N}] \\ [K_{21}][K_{22}][K_{23}]\dots[K_{2N}] \\ [K_{31}][K_{32}][K_{33}]\dots[K_{3N}] \\ \vdots\vdots\ddots\vdots \\ [K_{N1}][K_{N2}][K_{N3}]\dots[K_{NN}] \end{bmatrix} \begin{Bmatrix} \{D_1\} \\ \{D_2\} \\ \{D_3\} \\ \vdots \\ \{D_N\} \end{Bmatrix} = \begin{Bmatrix} \{F_1\} \\ \{F_2\} \\ \{F_3\} \\ \vdots \\ \{F_N\} \end{Bmatrix} \quad (5)$$

where $\{D_i\}$ and $\{F_i\}$ indicate displacement variables and loading and moments caused by the stresses and external forces acting on sphere i, respectively. The stiffness submatrices $[K_{ij}]\ |_{i=j}$ depend on the material properties of sphere i, and $[K_{ij}]\ |_{i\neq j}$ is defined by the contacts between spheres i and j. The equilibrium equations for each time step are derived by minimizing the total potential energy. The total potential energy Π is the summation over all potential energy forms calculated as below [1]:

$$\Pi = \pi_e + \pi_{is} + \pi_p + \pi_b + \pi_i + \pi_C + \pi_n + \pi_s + \pi_f \quad (6)$$

where π_e= the potential energies due to disk stiffness; π_{is}= the potential energy due to initial stress; π_p= the potential energy due to point loading;π_b= the potential energy due to body force; π_i= the potential energy due to inertia forces; π_C= the potential energy due to constrained spring; π_n= the potential energy due to normal contact; π_s= the potential energy due to shear contact; and π_f= the potential energy due to friction force.

The simultaneous equations are derived by minimizing the total potential energy Π of the disk system:

$$[K_{ij}] = \frac{\partial^2 \Pi}{\partial d_{ir}\partial d_{js}}, r, s = 1,2,3$$
$$\{F_i\} = -\frac{\partial \Pi(0)}{\partial d_{ir}}, r = 1,2,3 \quad (7)$$

where 0 refers to the initial state of each time state.

III. COMPARISON BETWEEN THE PENALTY METHOD AND ALM

The main features of the penalty method are [47]:

- There are no extra equations required by enforcement of constraints.
- The solution can easily be obtained by simply adding contact components to the stiffness matrix.
- The contact solution depends highly on the choice of the penalty number. The constraints are only satisfied in an approximate manner, and the optimal number cannot be explicitly found beforehand.
- If the penalty number is too large, the simultaneous equilibrium matrix becomes difficult to solve. However, the constraints are poorly satisfied if it is too low.

The ALM uses penalty stiffness but iteratively updates the contact traction to impose the contact constraints with a specified precision. The main features of this method are:

- In this method, no additional equations are required.
- In order to avoid the ill conditioning of the stiffness matrices, large penalty values are not required. Nevertheless, if the initial penalty number is too small, a large number ofiterations isrequired.
- The constraints are satisfied within a user-defined required tolerance.

IV. CONTACT MECHANICS USING ALM

In the penalty method, when a sphere-sphere or sphere-boundary contact occurs, the normal spring with a stiffness of P_n is introduced into the formulation to return the point to the surface along the shortest distance.

As shown in Figure 1, assume $P_1(x_1, y_1, z_1)$ indicates the location of the reference point of sphere i before a displacement increment and P_1^* represents the location after the displacement increment. The point$P_0(x_0, y_0, z_0)$ represents the projection of point P_1 on the reference plane S and P_0^* indicates this point after the displacement increment. Moreover, assume (u_1, v_1, w_1) and (u_0, v_0, w_0) are the displacement increments of points P_1 and P_0, respectively, and the unit normal vector of the reference plane S is $\hat{\boldsymbol{n}}$.

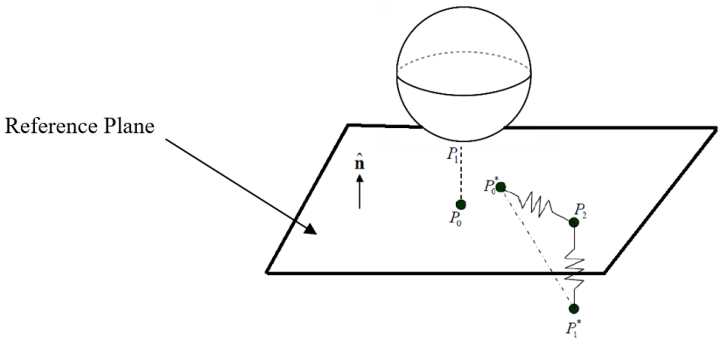

Fig.1. Sphere-sphere and sphere-boundary contacts(adapted from Beyabanaki and Bagtzoglou[1])

When using the ALM, the contact force at the contact point can be accurately approximated by iteratively calculating the Lagrange multiplier λ^*. A first-order updated value for λ^* can be written as follows:

$$\lambda \approx \lambda_{l+1}^* = \lambda_l^* + P_n . d_n \tag{8}$$

where the penalty number,P_n, can be variable and does not have to be a very large number as in the penalty method. In Equation (8), λ_l^* is the Lagrange multiplier at the l-th iteration and λ_{l+1}^* is the updated Lagrange multiplier, and the normal distance d_n of point P_1^* from the reference plane S is:

$$d_n = M + [H_i]\{D_i\} - [Q_j]\{D_j\} \tag{9}$$

where

$$M = \hat{\boldsymbol{n}} . \begin{bmatrix} x_1 - x_0 \\ y_1 - y_0 \\ z_1 - z_0 \end{bmatrix} \tag{10}$$

$$[H_i] = \hat{\boldsymbol{n}} . T_i(x_1, y_1, z_1) \tag{11}$$

$$[Q_j] = \hat{\boldsymbol{n}} . T_j(x_0, y_0, z_0) \tag{12}$$

At the l-th iteration, the potential energy resulting from the contact force is calculated as follows:

$$\pi = \lambda_l^* \ d_n + \frac{1}{2} P_n {d_n}^2 \tag{13}$$

Equation (13) consists of two components. The first component is the strain energy resulting from the iterativeLagrange multiplier λ_l^* , and the penalty constraint creates the second. The contribution of the second component to the simultaneous equilibrium equations was already derived by Beyabanaki and Bagtzoglou [1].

The first component of Equation (13) can be written as:

$$\pi^* = \lambda_l^* \left(\frac{M}{l} + [H_i][D_i] - [Q_j][D_j] \right) \tag{14}$$

The derivatives of $\pi^*$with respect to $d_{ki}$and d_{kj} at zero are:

$$f_{ki} = -\frac{\partial \pi^*(0)}{\partial d_{ki}} \tag{15}$$

$$f_{kj} = -\frac{\partial \pi^*(0)}{\partial d_{kj}} \tag{16}$$

where 0 refers to the initial state of each time state. They form the following submatrices:

$$f_{ki} = -\lambda_l^* . [H_i] \tag{17}$$

$$f_{kj} = -\lambda_l^* . [Q_j] \tag{18}$$

For the ALM, the combined contribution of the first and second components of Equation (13) to the simultaneous equilibrium equation is summarized below.

The following matrices can be added to submatrices $[K_{ii}]$, $[K_{ij}]$, $[K_{ji}]$, and $[K_{jj}]$ in the global stiffness matrix:

$$[K_{ii}] = P_n[H_i]^T[H] \tag{19}$$

$$[K_{ij}] = P_n[H_i]^T[Q_j] \tag{20}$$

$$[K_{ji}] = P_n[Q_j]^T[H_i] \tag{21}$$

$$[K_{jj}] = P_n[Q_j]^T[Q_j] \tag{22}$$

and the following vectors are calculated and then added to the global force vector:

$$[F_i] = -(\lambda_l^* + P_n\frac{M}{l}).[H_i]^T \tag{23}$$

$$[F_i] = -(\lambda_l^* + P_n\frac{M}{l}).[Q_j]^T \tag{24}$$

The final exact contact forces can always be obtained by the iterative method, even with small initial values of the penalty number. The iterative procedure for the ALM is presented in Figure2.

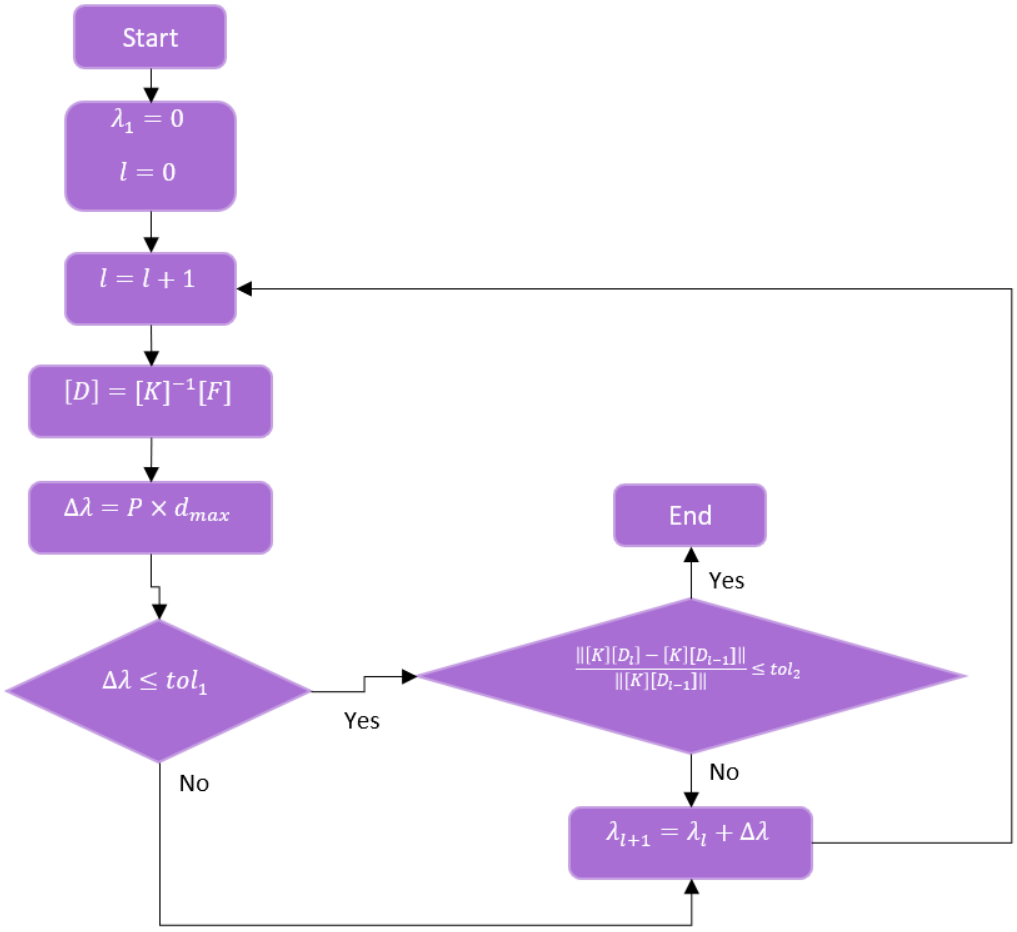

Fig.2. Flowchart of ALM procedure used in sphere-based 3-D DDA

V. EXAMPLE 1: FUNNEL FLOW

To investigate the proposed contact mechanics, an example of funnel flow is presented, and the results are compared with the results obtained by using the penalty method in the original formulation.

As shown in Figure 3, there are two layers of spheres with different sizes above a funnel that travel vertically because of gravity. Each disk has a density of $2500\ kg/m^3$; and the stiffness of the normal contact spring, the time step size, and the friction angle are $P = 1 \times 10^5 N/m$, $0.01s$ and 5°, respectively. Figures 4 and 5 show the configuration of spheres after 6s and 8.6s using the penalty method and the ALM, respectively. As

can be seen, when using the ALM, no sphere interpenetration occurs, even though the initial penalty number is low. However, without the ALM, there is contact overlap and interpenetration.

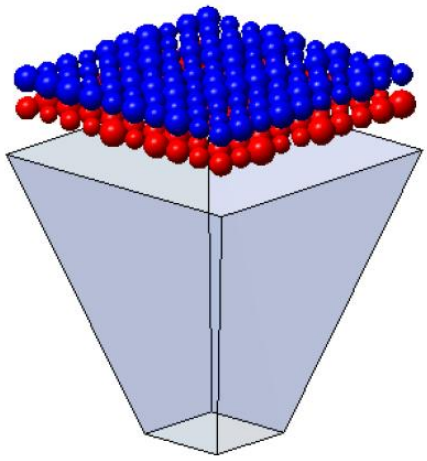

Fig.3. Initial configuration of the funnel system

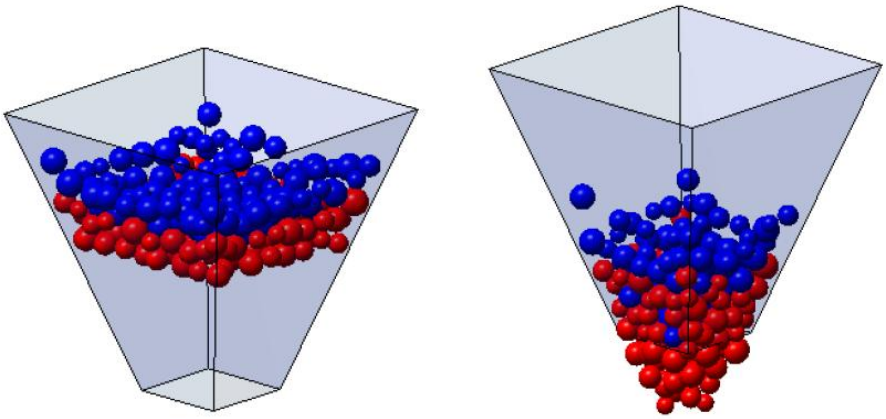

(a) (b)

Fig.4. Results of sphere-based 3-D DDA using the ALM: (a) after 6s, (b) after 8.6s

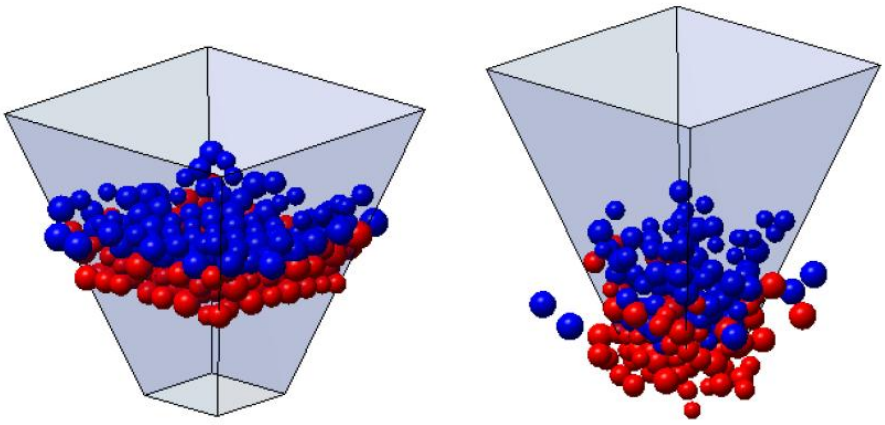

(a) (b)

Fig.5. Results of sphere-based 3-D DDA using the penalty method: (a) after 6s, (b) after 8.6s

VI. EXAMPLE 2: MULTIPLE SLOPES

The example used to test the original developed contact theory for sphere-based 3-D DDA (Beyabanaki and Bagtzoglou [1]) is presented in this section, and the results are compared with the results obtained by using the penalty method in the original formulation.

This case is a landslide analogy. In this example, as shown in Figure 6, a slope including five inclined planes is considered. A total of 180 spheres rest on the highest inclined plane. Under the action of gravitational force, the spheres move on the planes. Density of the spheres is $3500\,kg/m^3$, and the stiffness of the normal contact spring and the time interval are assumed to be $P = 1 \times 10^4 kN/m$ and $0.05s$, respectively. Figures 7 and 8 show the configuration of spheres after 20s, 47s, and 63s using the penalty method and the ALM, respectively. As can be seen, the spheres move along the inclined planes without any violation of boundary constraints when the ALM is used. However, as shown in Figure 8, a small penalty number with the classical penalty method is unable to enforce the interpenetration constraint.

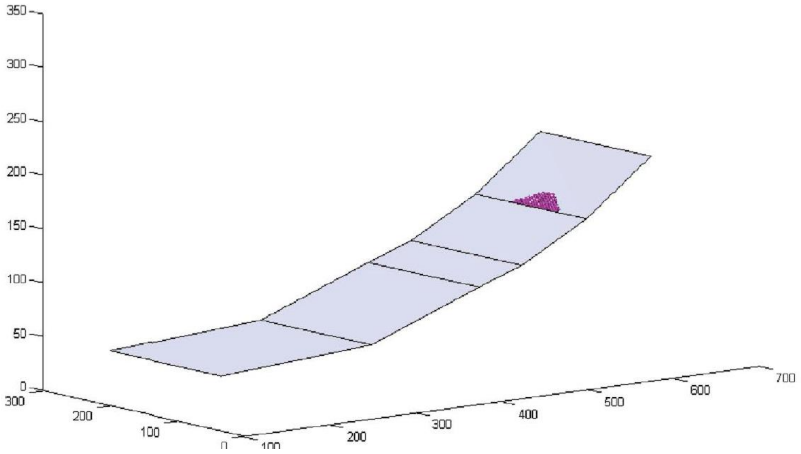

Fig.6. Initial configuration

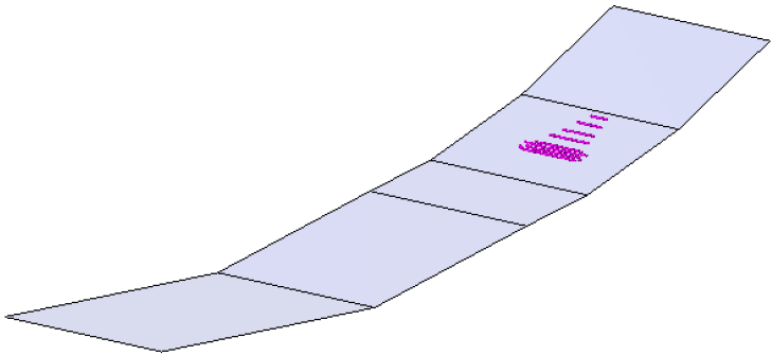

(a)

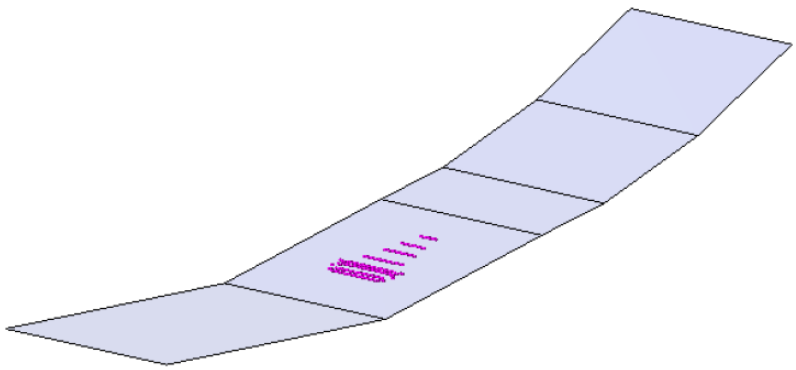

(b)

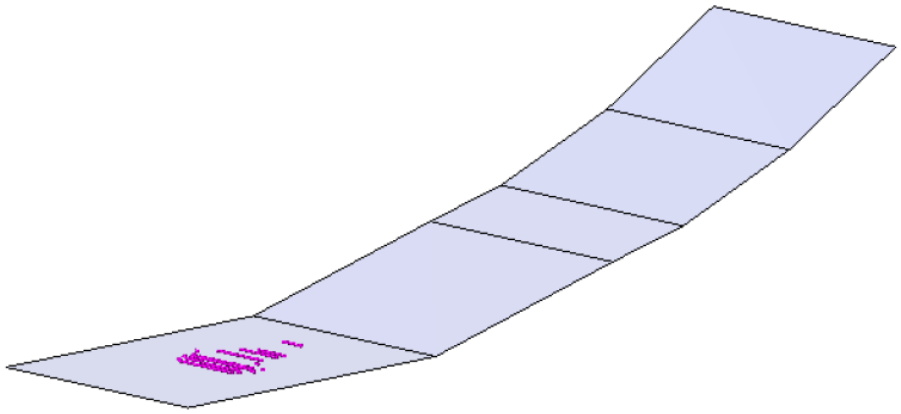

(c)

Fig.7. Results of sphere-based 3-D DDA using ALM: (a) after 20s, (b) after 47s (c) after 63s

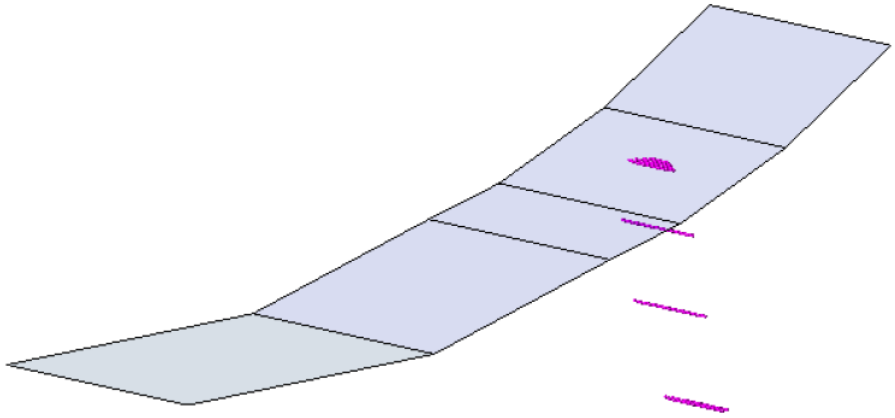

(a)

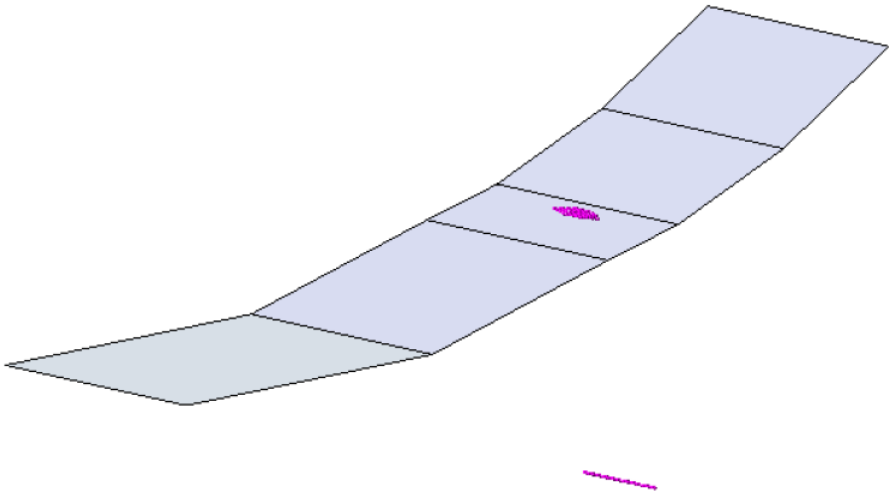

(b)

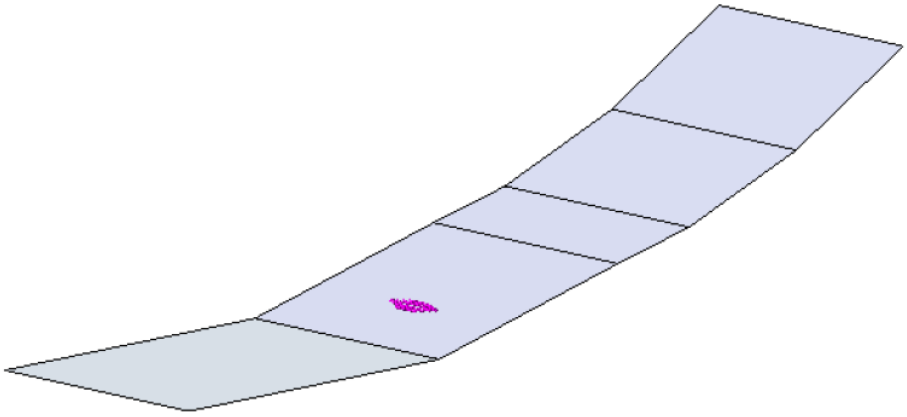

(c)

Fig.8. Results of sphere-based 3-D DDA using the Penalty method: (a) after 20s, (b) after 47s (c) after 63s

VII. CONCLUSIONS

In the existing sphere-based 3-D DDA method, the contact constraints are enforced using the penalty method. The contact solution depends highly on the choice of the penalty number in this approach. Also, the optimal number cannot be explicitly found beforehand. If the penalty number is too low,the constraints are either not met or poorly satisfied. However, if the number is too large, the simultaneous equilibrium equations become difficult to solve. Therefore, it is important to use the ALM approach. In this paper, contact constraints are enforced using the ALM and two illustrative examples are presented to demonstrate the new model. Using the ALM to enforce contact restraints retains the simplicity of the penalty method and reduces its disadvantages.

REFERENCES

[1]. Beyabanaki SAR and Bagtzoglou AC. 2012. Three-dimensional discontinuous deformation analysis (3-D DDA) method for particulate media applications, Geomechanics and Geoengineering: An International Journal, 7(4): 239–253.

[2]. Shi GH. 1988. Discontinuous deformation analysis: a new numerical model for the statics and dynamics of block systems. PhD thesis, Department of Civil Engineering, University of California, Berkeley.

[3]. Shi GH. 1993. Block System Modeling by Discontinuous Deformation Analysis. Computational Mechanics Publication: Southampton. UK.

[4]. Jing L, Hudson JA. 2002. Numerical methods in rock mechanics. International Journal of Rock Mechanics & Mining Sciences, 39: 409–427.

[5]. Jing L. 2003. A review of techniques, advances and outstanding issues in numerical modelling for rock mechanics and rock engineering. International Journal of Rock Mechanics & Mining Sciences, 40: 283–353.

[6]. Ohnishi Y, Nishiyama S. 2007. Recent insights of analyses using discontinuous methods in rock engineering in Japan. Proceedings of the 8th International Conference on Analysis of Discontinuous Deformation: Fundamentals and Applications to Mining and Civil Engineering, Beijing, China, August 14-19, 15–26.

[7]. MacLaughlin MM, Doolin DM. 2006. Review of validation of the discontinuous deformation analysis (DDA) method. Int J Numer Anal Meth Geomech, 30: 271–305.

[8]. Shi GH. 2007. Applications of discontinuous deformation analysis (DDA) to rock stability analysis. Proceedings of the 8th International Conference on Analysis of Discontinuous Deformation: Fundamentals and Applications to Mining and Civil Engineering, Beijing, China, August 14–19, 1–13.

[9]. Hatzor YH and Bakun-Mazor D. 2011. Modeling dynamic deformation in natural rock slopes and underground openings with DDA: Review of recent results. Geomechanics and Geoengineering: An International Journal, 6(4):283–292.

[10]. Shi GH. 2001. Three dimensional discontinuous deformation analysis. Proceedings of the 38th US Rock Mechanics Symposium, D Elsworth et al., ed., 1421–1428.

[11]. Wu JH, Ohnishi Y, Shi GH, Nishiyama S. 2005. Theory of three-dimensional discontinuous deformation analysis and its application to a slope toppling at Amatoribashi, Japan. International Journal of Geomechanics, 179–195.

[12]. Liu J, Kong X, Lin G. 2004. Formulation of the three-dimensional discontinuous deformation analysis method. Acta MechanicaSinica, 20(3): 270–282.

[13]. Yeung MR, Jiang QH, Sun N. 2003. Validation of block theory and three-dimensional discontinuous deformation analysis as wedge stability analysis method. Int J Rock Mech Min Sci, 40(2): 265–275.

[14]. Yeung MR, Sun N, Jiang QH, Blair SC. 2004. Analysis of large block test data using three-dimensional discontinuous deformation analysis. Int J Rock Mech Min Sci, 41(3): 458–459.

[15]. Jiang QH, Yeung MR. 2004. A model of point-to-face contact for three-dimensional discontinuous deformation analysis. Rock Mechanics and Rock Engineering, 37(2):95–116.

[16]. Wu JH, Juang CH, Lin HM. 2005. Vertex-to-face contact searching algorithm for three-dimensional frictionless contact problems. International Journal for Numerical Methods in Engineering, 63(6): 876–897.

[17]. Yeung MR, Jiang QH, Sun N. 2007. A model of edge-to-edge contact for three-dimensional discontinuous deformation analysis. Computers and Geotechnics, 34(3): 175–186.

[18]. Wu JH. 2008. New edge-to-edge contact calculating algorithm in three-dimensional discrete numerical analysis. Advances in Engineering Software, 39(1): 15–24.

[19]. Beyabanaki SAR, Grayeli R, Hatami K. 2008. Three-dimensional discontinuous deformation analysis (3-D DDA) using a new contact resolution algorithm. Computers and Geotechnics, 35: 346-356.
[20]. Ahn TY, Song JJ. 2011. New contact-definition algorithm using inscribed spheres for 3D discontinuous deformation. International Journal of Computational Methods, 8(2): 171–191.
[21]. Beyabanaki SAR, Jafari A, Biabanaki SO, Yeung MR. 2009. A coupling model of 3-D discontinuous deformation analysis (3-D DDA) and finite element method, AJSE, 34:2B: 107–119.
[22]. Beyabanaki SAR, Jafari A, Biabanaki SO, and Yeung MR. 2009. Nodal-based three-dimensional discontinuous deformation analysis (3-D DDA), Computers and Geotechnics, 36: 359–372.
[23]. Beyabanaki SAR, Jafari A, Yeung MR. 2009d. Second-order displacement functions for three-dimensional discontinuous deformation analysis (3-D DDA), International Journal of Science and Technology, 16(3): 216–225.
[24]. Beyabanaki SAR, Jafari A, and Yeung MR. 2010. High-order three-dimensional discontinuous deformation analysis (3-D DDA). International Journal for Numerical Methods in Biomedical Engineering, 26 (12): 1522–1547.
[25]. Liu J, Nan Z, Yi P. 2012. Validation and application of three-dimensional discontinuous deformation analysis with tetrahedron finite element meshed block. Acta MechanicaSinica, 28(6): 1602–1616.
[26]. Beyabanaki SAR, Ferdosi B, Mohammadi S. 2009. Validation of dynamic block displacement analysis and modification of edge-to-edge contact constraints in 3-D DDA. International Journal of Rock Mechanics and Mining Sciences, Elsevier, 46: 1223–1234.
[27]. Bakun-Mazor D, Hatzor YH, Glaser SD. 2012. Dynamic sliding of tetrahedral wedge: The role of interface friction. International Journal for Numerical and Analytical Methods in Geomechanics, 36(3): 327–343.
[28]. Zhang H, Chen G, Zheng L, Zhang Y, Wu YQ, Han Z, Fan FS, Jing PD, Wang W. 2014. A new discontinuous model for three dimensional analysis of fluid-solid interaction behavior. In: Proceedings of the TC105 ISSMGE International Symposium on Geomechanics from Micro to Macro, Cambridge, UK, 1-3 September 2014:1-6.
[29]. Zhu, H. H., W. Wu, J. Q. Chen, G. W. Ma, X. G. Liu, and X. Y. Zhuang. 2016. Integration of three dimensional discontinuous deformation analysis (DDA) with binocular photogrammetry for stability analysis of tunnels in blocky rock mass. Tunnelling Underground Space Technol. 51(Jan): 30–40.
[30]. Zhao, G., J. Lian, A. Russell, and J. Zhao. 2017. Three-dimensional DDA and DLSM coupled approach for rock cutting and rock penetration. Int. J. Geomech. 17 (5): E4016015.
[31]. Zhang, H., S. G. Liu, W. Wang, L. Zheng, Y. B. Zhang, Y. Q. Wu, Z. Han, Y. G. Li, and G. Q. Chen. 2018. A new DDA model for kinematic analyses of rockslides on complex 3-D terrain. Bull. Eng. Geol. Environ. 77 (2): 555–571.
[32]. Liu SG, Z. J. Li, H. Zhang, W. Wu, G. H. Zhong, and S. Lou. 2018. A 3-D DDA damage analysis of brick masonry buildings under the impact of boulders in mountainous areas. J. Mt. Sci. 15 (3): 657–671.
[33]. Beyabanaki SAR, 2019. Applications of Three-Dimensional Discontinuous Deformation Analysis: A Review, American Journal of Engineering Research (AJER), Vol. 8, No. 10, 237-245.
[34]. Ke, T.-C., and Bray, J. D. 1995.Modeling of particulate media using discontinuous deformation analysis. J. Eng. Mech., 121(11): 1234–1243.
[35]. Rein G, Andrés A. 2001. Computer simulation of granular material: Vibrating feeders. Powder Handling & Processing, 13(2): 181–185.
[36]. Thomas, PA, Bray, J. D. 1999. Capturing nonspherical shape of granular media with disk clusters. J Geotech Geoenviron. Eng, 125(3): 169–178.
[37]. Thomas, PA. 1997. Discontinuous deformation analysis of particulate media. PhD thesis, University of California, Berkeley, Berkeley, CA.
[38]. Koyama T, Nishiyama S, Yang M, Ohnishi Y. 2011. Modeling the interaction between fluid flow and particle movement with discontinuous deformation analysis (DDA) method. Int J Numer Anal Meth Geomech, 35: 1–20.
[39]. Beyabanaki SAR and Bagtzoglou AC. 2015. Sphere-boundary edge and sphere-boundary corner contacts model in DDA for simulating particulate media in 3-D, Geomechanics and Geoengineering: An International Journal, 10(2): 83–94.
[40]. Beyabanaki SAR and Bagtzoglou AC. 2013. Non-rigid disk-based DDA with a new contact model, Computers and Geotechnics, 49: 25–35.
[41]. Beyabanaki SAR and Bagtzoglou AC. 2014. Accuracy of dynamic disk-based DDA with respect to a single sliding disk cluster. Geomechanics and Geoengineering: An International Journal, 9(3): 231–240.
[42]. Beyabanaki SAR, Bagtzoglou AC, Liu L, 2016. Applying disk-based discontinuous deformation analysis (DDA) to simulate Donghekou landslide triggered by the Wenchuan earthquake. Geomechanics and Geoengineering: An International Journal, 11(3): 231–240.
[43]. Huang GH, Jiao YY, Wang L, Zhao Q. 2017. Three-Dimensional Spherical DDA Method for Modeling Friction Problems. International Journal of Geomechanics, 5:1-9.
[44]. Wang L, Jiao YY, Huang GH, Zheng F, Zhao Q. 2017. Model of Sphere-to-Edge Contact for Spherical Discontinuous Deformation Analysis. International Journal of Geomechanics, 17(12):1-10.
[45]. Fan H, Huang D, Wang G, Jin F, 2020. Discontinuous deformation analysis for ellipsoids using cone complementary formulation, Computers and Geotechnics, 121, in press.
[46]. Liu X, 2016. Augmented Lagrangian method for total generalized variation based Poissonian image restoration. Computers & Mathematics with Applications, 71(8): 1694–1705.
[47]. Mohammadi S, 2003. Discontinuous Mechanics using Finite and Discrete elements. WIT Press.

S. Amir Reza Beyabanaki,etal."Modified Contact Constraints in Sphere-Based 3-D DDA." *American Journal of Engineering Research (AJER)*, vol. 9(04), 2020, pp. 171-180.